

# PCCP

Accepted Manuscript



This is an *Accepted Manuscript*, which has been through the Royal Society of Chemistry peer review process and has been accepted for publication.

*Accepted Manuscripts* are published online shortly after acceptance, before technical editing, formatting and proof reading. Using this free service, authors can make their results available to the community, in citable form, before we publish the edited article. We will replace this *Accepted Manuscript* with the edited and formatted *Advance Article* as soon as it is available.

You can find more information about *Accepted Manuscripts* in the [Information for Authors](#).

Please note that technical editing may introduce minor changes to the text and/or graphics, which may alter content. The journal's standard [Terms & Conditions](#) and the [Ethical guidelines](#) still apply. In no event shall the Royal Society of Chemistry be held responsible for any errors or omissions in this *Accepted Manuscript* or any consequences arising from the use of any information it contains.

## ARTICLE

# Advanced unidirectional photocurrent generation via cytochrome *c* as reaction partner for directed assembly of photosystem I

Cite this: DOI: 10.1039/x0xx00000x

Kai R. Stieger,<sup>a</sup> Sven C. Feifel<sup>a</sup>, Heiko Lokstein<sup>b</sup> and Fred Lisdat<sup>a</sup>Received 00th January 2012,  
Accepted 00th January 2012

DOI: 10.1039/x0xx00000x

www.rsc.org/

Conversion of light into an electrical current based on biohybrid systems mimicking natural photosynthesis is becoming increasingly popular. Photosystem I (PSI) is particularly useful in such photo-bioelectrochemical devices. Herein, we report on a novel biomimetic approach for an effective assembly of photosystem I with the electron transfer carrier cytochrome *c* (cyt *c*), deposited on a thiol-modified gold-surface. Atomic force microscopy and surface plasmon resonance measurements have been used for characterization of the assembly process. Photoelectrochemical experiments demonstrate a cyt *c* mediated generation of an enhanced unidirectional cathodic photocurrent. Here, cyt *c* can act as a template for the assembly of an oriented and dense layer of PS I and as wiring agent to direct the electrons from the electrode towards the photosynthetic reaction center of PSI. Furthermore, three-dimensional protein architectures have been formed via the layer-by-layer deposition technique resulting in a successive increase in photocurrent densities. An intermittent cyt *c* layer is essential for an efficient connection of PSI layers with the electrode and for an improvement of photocurrent densities.

## Introduction

Artificial systems exploiting the features of natural photosynthesis are increasingly becoming a focus of current research.<sup>1,2</sup> Particularly the two photosystems (PS) of the oxygenic photosynthesis have attracted the attention of researchers to build up new biohybrid solar energy-converting systems.<sup>3,43,44</sup> In photosystem I (PSI) absorption of light results in charge separation with a quantum efficiency of nearly unity.<sup>4</sup> Moreover, PSI can be readily isolated from plants and cyanobacteria with a high yield, thus PSI is frequently used as a

natural resource in biohybrid light converting entities.<sup>5-7</sup> In such systems efficient coupling of PSI with electrodes is essential. Besides the light-to-current conversion, PSI may also be used for light-driven redox and/or enzymatic reactions.

In the thermophilic cyanobacterium *Thermosynechococcus elongatus* (*T. elongatus*), PSI is a trimeric pigment-protein super-complex with 12 different protein subunits, harboring 96 chlorophylls *a* (Chl *a*) – per monomeric subunit. Most Chls serve as light-harvesting antenna pigments and 6 Chls form the electron transport chain.<sup>8</sup> Electron transfer in PSI starts at a luminal pigment dimer, Chl *a*/Chl *a*' (P700) finally leading to a reduction of the stromal-located terminal iron-sulfur-cluster (F<sub>B</sub>).<sup>6,7</sup>

To date several approaches of coupling PSI to gold surfaces have been described. One of them is the covalent fixation of PSI, which has been achieved mainly via amino-reactive surface chemistry in order to obtain fixation and a short distance of the reaction center to the electrode for direct electron transfer (DET).<sup>9,10</sup> Improvements in surface enlargements by using meso- and nanostructured surfaces have been reported, for example coupling PSI with gold-nanoparticles<sup>11</sup> and on nanoporous gold leaves<sup>10</sup>. A molecular wiring approach have been accomplished by reconstitution of PSI with vitamin K<sub>1</sub> derivatives.<sup>12</sup> Application of crosslinked Platinum-nanoparticle/PSI composites with ferredoxin<sup>13</sup> or pyrroloquinoline quinone-linked PSI as a biohybrid relay assembly<sup>32</sup> have also been reported. Additionally, PSI has been assembled in a non-covalent fashion onto different self-assembling monolayers (SAM) with terminal carboxy-, hydroxy- or amino-functions via adsorption.<sup>14-19,40</sup> Nevertheless, DET from PSI to a transducer results rather often in minor photocurrent densities, mainly due to long electron tunneling distances between the reaction center and the

electrode. Owing to the embedding of PSI in an Osmium-complex containing redox polymer such issues as long electron transfer distances and low active protein density have been overcome.<sup>20</sup> Recent investigations also address indirect electron transfer (IET) with various combinations of redox mediators in solution.<sup>21</sup> However, in general current approaches result in photocurrent densities, which are orders of magnitude lower than those predicted by theoretical calculations, in particular, taking into account the high quantum efficiency of PSI, the fast intramolecular rate of charge separation ( $< 1 \mu\text{s}$ ) and assuming an optimal PSI surface coverage of  $0.5 \text{ pmol cm}^{-2}$ .<sup>12,22</sup> One reason is related to the lack of controlled orientation of PSI on the electrode surface<sup>23</sup>, another may be the limited accessibility of mediator molecules to PSI.<sup>21</sup>

In the present work, we use cytochrome *c* (cyt *c*) as a tool for the assembly of PSI. The electrochemistry of this small redox protein ( $\sim 12 \text{ kDa}$ ) and the adsorption processes onto modified gold-electrodes are quite well understood.<sup>29-31</sup> Very recently, a similar attempt has been accomplished using a cyt *c* polymer complex to connect PSI to an electrode.<sup>26</sup> In this study, we apply a different strategy by coupling cyt *c* via self-assembling monolayers, which provides a very stable and efficient electrical connection of cyt *c* with the electrode. We also address detailed investigations on the conditions under which cyt *c* can act as a protein scaffold for a non-covalent assembly of PSI, e. g. pH of buffer, PSI concentration and time period. Atomic force microscopy is used to elucidate the complex surface structure of the cyt *c* – PSI bilayer formation. Furthermore the capability for an efficient electron transfer in a surface-fixed state is explored, resulting in a unidirectional generation of photocurrents. In addition, we demonstrate a next step of development by building-up three dimensional cyt *c*/PSI architectures in order to obtain enhanced photocurrent densities. This novel approach displays the potential of cyt *c* to act as molecular protein scaffold for connecting PSI with electrodes, even if the biomolecules are immobilized rather far from the electrode surface.

## Experimental

### Isolation of Photosystem I from *T. elongatus*

Trimeric PSI has been isolated from *T. elongatus* essentially as described previously.<sup>38,39</sup> The PSI containing fraction has been further purified by one or two sucrose gradient ultracentrifugation steps as required. Functionality of PSI has been assessed as light-driven electron transport from ascorbate-reduced 2,6-dichloroindophenol to methyl viologen (1,1'-dimethyl-4,4'-bipyridinium,  $\text{MV}^{2+}$ ) with a Clark-type electrode (Oxyview-1, Hansatech, King's Lynn, UK). Typical light-induced oxygen consumption rates were on the order of  $3.5 \mu\text{mol mg}^{-1} \text{ Chl } a * \text{min}^{-1}$ . Fluorescence emission spectra measured at RT and 77 K indicated the integrity of the excitation energy transfer chain in PSI.

### Preparation of Au-SAM/cyt *c*/PSI mono- and multilayer electrodes

Au-rod-electrodes (CHI) with an accessible geometrical surface of  $0.0314 \text{ cm}^2$  have been cleaned with abrasive paper (P1200, P2500, P3000) and subsequently cycled between  $-0.2$  and  $1.6 \text{ V}$  (vs. Ag/AgCl) in  $100 \text{ mM}$  sulfuric acid. Followed by an incubation for 48 h at RT with an ethanolic solution of a 3:1 mixture containing 11-mercapto-1-undecanol (MU, Sigma) and 11-mercaptopundecanoic acid (MUA, Sigma). Afterwards the electrode has been incubated with  $30 \mu\text{M}$  cytochrome *c* (horse heart, Sigma) in phosphate buffer ( $5 \text{ mM}$ , pH 7) for 2 h. Subsequently the Au-SAM/cyt *c* electrodes have been incubated in the dark with purified  $0.2 \mu\text{M}$  PSI trimer in phosphate buffer ( $5 \text{ mM}$ , pH 7) over night at  $4 \text{ }^\circ\text{C}$  and were finally ready for measurements.

In multilayer preparations the Au-SAM/cyt *c*/PSI electrodes have been alternately incubated with  $30 \mu\text{M}$  cyt *c* solution for 2 h at RT and  $0.2 \mu\text{M}$  PSI trimer solution for 2 h at RT in phosphate buffer ( $5 \text{ mM}$ , pH 7). At all incubation stages cyclic voltammograms have been recorded to verify the assembly process.

### Electrochemical experiments

Electrochemical measurements have been performed using a potentiostat (Zennium, Zahner) and an electrochemical cell containing 5 mL of a phosphate buffer ( $5 \text{ mM}$ , pH 7) a Pt counter electrode and an Ag/AgCl ( $3 \text{ M KCl}$ ) reference electrode. Cyclic voltammetric measurements have been performed at a scan rate of  $100 \text{ mV s}^{-1}$  and in a potential range from  $+300$  to  $-300 \text{ mV}$ .

### Photoelectrochemical experiments

Photoelectrochemical measurements have been performed using an integrated system (CIMPS, Zahner) containing a white LED light source ( $4300 \text{ K}$ , Zahner) with a continuous change of intensity (max.  $100 \text{ mW cm}^{-2}$ ), an electrochemical cell and a photodiode with feedback control to the light source via a potentiostat (PP211, Zahner). Electrochemical investigations have been carried out through a coupled potentiostat (Zennium, Zahner). In all experiments a Pt counter electrode and an Ag/AgCl ( $3 \text{ M KCl}$ ) reference electrode have been used in an aqueous solution containing phosphate buffer ( $5 \text{ mM}$ , pH 7). As a soluble electron mediator  $\text{MV}^{2+}$  has been used at a final concentration of  $250 \mu\text{M}$ . Photochronoamperometric experiments have been performed at RT and different potentials ( $-100 \text{ mV}$ ,  $200 \text{ mV}$ ,  $500 \text{ mV}$  vs. Ag/AgCl), while using an illumination time of 30 s. Chopped light voltammetry experiments have been done at a scan rate of  $2 \text{ mV s}^{-1}$  from  $250 \text{ mV}$  to  $-300 \text{ mV}$  with a light intensity of  $60 \text{ mW cm}^{-2}$  and a light period time of 15 s.

### Atomic force microscopy

Atomic force microscopy (AFM) images have been taken in the quantitative imaging (QI) mode in phosphate buffer ( $5 \text{ mM}$ , pH 7) by the use of an atomic force microscope (Nanowizard 3, JPK) and a cantilever ( $0.7 \text{ N m}^{-1}$ , Bruker). In all experiments an unused planar gold-chip (Xantec) with an rms surface roughness of about  $0.2 - 0.4 \text{ nm}$  served as substrate. The new

Au surface has been incubated for 48 h at RT with a freshly prepared ethanolic solution of a 3:1 mixture containing MUA and MUA. After extensively washing the surface with ethanol and phosphate buffer (5 mM, pH 7) the chip first has been incubated for 2 h at RT with 30  $\mu\text{M}$  cyt *c* in phosphate buffer (5 mM, pH 7) and second treated with 0.2  $\mu\text{M}$  PSI in phosphate buffer (5 mM, pH 7) over night in the dark at 4 °C. At all incubation stages AFM-images have been taken.

### Surface plasmon resonance

Surface plasmon resonance (SPR) experiments have been performed on a Biacore T100 (GE Healthcare) at a constant flow rate of 1  $\mu\text{L min}^{-1}$  and 25 °C. Before use, Au sensor chips have been cleaned with a low pressure air plasma. The clean Au surface has been incubated 48 h at RT with a freshly prepared ethanolic solution of a mixture containing MUA and MU. After the thorough washing of the surface with ethanol and phosphate buffer (5 mM, pH 7) the chip was ready to use. First cyt *c* has been adsorbed on the thiol layer and subsequently PSI solutions of different pH and concentration have been flushed over the surface.

## Results and Discussion

### Assembly of photosystem I on cytochrome *c*

In a first attempt, the non-covalent assembly of PSI on a cyt *c* monolayer (cyt *c* ML) has been investigated. This idea is based on the natural situation in which plastocyanine or cyt *c6* can act as an electron donor of PSI.<sup>24,25</sup> In addition, it has been shown that cyt *c6* can mediate the reactivity of PSI with electrodes in solution.<sup>27</sup> *T. elongatus*-PSI has a luminal-located binding site close to P700 suited for cyt *c6* interaction.<sup>6</sup> Although cyt *c* from horse heart is rather different from cyt *c6*, it provides the advantages of fast reactions at electrodes and a high isoelectric point<sup>28</sup> (10 – 10.5), which leads to a pronounced electrostatic adsorption on negatively charged SAMs and may also support an improved interaction with PSI.

Hence, we have investigated the assembly process of PSI on a cyt *c* layer by surface plasmon resonance (SPR). The sensorgram in Fig. 1 demonstrates the assembly of PSI on a

**Fig. 1** Surface plasmon resonance (SPR) sensorgram of the assembly of cyt *c* and PSI on modified gold surfaces. (a) Deposition of cyt *c* on a SAM-modified gold surface, (b) Deposition of PSI on a SAM-modified gold surface and (c) Deposition of PSI on SAM-modified gold surface after deposition of cyt *c*. All experiments have been performed in phosphate buffer (5 mM, pH 7) in a flow system (1  $\mu\text{L min}^{-1}$ ). A mixture of 11-mercaptoundecanoic acid (MUA) and 11-mercapto-1-undecanol (MU) (1:3) have been used as SAMs for modification of the gold surface prior to the protein assembly.

MUA/MU-modified gold-surface (see experimental section) with and without a subjacent cyt *c* monolayer. First a rather fast adsorption of cyt *c* on the MUA/MU-SAM is observed. This results in a surface concentration of  $15 \pm 1 \text{ pmol cm}^{-2}$  ( $n = 5$ ), which reflects well the protein amount detected via electrochemistry: from cyclic voltammetric experiments (CV)

the cyt *c* surface concentration can be calculated to be  $14 \pm 0.8 \text{ pmol cm}^{-2}$  ( $n = 9$ ), which is in agreement with other studies described previously.<sup>29-31</sup>

The successful adsorption of PSI by injections on top of a cyt *c* ML can also be shown. In this experiment three subsequent PSI injections with intermittent buffer wash have been used in order to grant the system enough time for proper rearrangement on the surface and test for a potentially protein desorption (see Fig. 1). Given that 3 injection steps of PSI (2 min each) still result in a further mass increase, it can be concluded, that PSI exhibits a rather slow binding kinetics to the cyt *c* ML compared to the cyt *c* binding to MUA/MU. When PSI is flushed over a MUA/MU-modified surface a comparable slow adsorption behavior can be seen. However, a significantly reduced mass deposition is detected, demonstrating the importance of a subjacent cyt *c* ML for an efficient PSI assembly process.

Further SPR experiments without intermittent buffer flow have been performed evaluating the best conditions for PSI adsorption onto a cyt *c* ML. When PSI is assembled with a concentration of 0.2  $\mu\text{M}$  in a buffer with low ionic strength (5 mM phosphate buffer) at pH 7 most efficient protein deposition can be observed. Higher and lower concentrations of trimeric PSI lead to a significant reduction of the assembly rate (see Fig. s1, ESI). Deposition experiments of PSI from a storage buffer (50 mM TRIS, 0.04 %  $\beta$ -dodecyl-maltoside ( $\beta$ -DM), pH 8) also exhibits less mass accumulation due to the interaction of the detergent  $\beta$ -DM with the surface. Hence, a buffer exchange to low ion concentrations and a removal of  $\beta$ -DM have been performed.

A surface saturation with PSI can be achieved after an incubation time of 1 h resulting in a surface concentration of approximately 1  $\text{pmol cm}^{-2}$  (see Fig. s2A, ESI). For PSI binding electrostatic forces are dominant at pH 7, due to a positive excess net-charge of cyt *c* and a prominent negative net-charge at the luminal side of PSI (see Fig. s3, ESI).<sup>34-37,40</sup> A study of the pH-influence in the PSI deposition process on a cyt *c* ML, indicates clearly that a pH variation ranging from 8 to 6.5, has a quite strong impact on the PSI adsorption. This is due to the change in charge distribution on the protein surface (see Fig. s1A, ESI).

In order to confirm the deposition of PSI, AFM-measurements have been performed and are shown in Fig. 2.

**Fig. 2** Atomic force microscopy (AFM) images of cyt *c*/PSI assemblies on Au-SAM substrates. (a) AFM image of cyt *c* adsorbed to a SAM of MUA, MU (Au-SAM/cyt *c*). (b) AFM image of a PSI assembly on top of a cyt *c* monolayer (Au-SAM/cyt *c*/PSI). (c) Corresponding cross section graph of Au-SAM/cyt *c* (dashed) and Au-SAM/cyt *c*/PSI (solid) with a total line width of 1  $\mu\text{m}$ . In (a) and (b) the color scale is shown on the top of the Fig., ranging from 0 to 22 nm.

Because of the small size of cyt *c* and the formation of a densely packed monolayer, a rather low roughness can be found for the surface with the redox protein only. The PSI deposition however, changes the AFM-image compared to the cyt *c* layer displaying a dense structure with small gap-sections. Cross-

section analysis has been carried out to elucidate the roughness-parameter for better comparison. The rms roughness for the *cyt c*-modified surface is about  $0.3 \pm 0.1$  nm ( $n = 3$ ). The roughness-value changes by one order of magnitude to  $3.5 \pm 0.2$  nm ( $n = 3$ ) for the deposition of PSI. The profile given in Fig. 2c and the increased roughness obviously confirm the deposition of a complete and rather compact layer of PSI. Additionally this is in very good agreement with the rather high surface concentrations found in SPR experiments.

### Photocurrent generation of Au-SAM/*cyt c*/PSI electrodes

After verifying the successful assembly of trimeric PSI on *cyt c*-modified Au-surfaces, the functional properties of these *cyt c*/PSI systems have been investigated. First, we characterize the electrochemical properties of the *cyt c* layer with and without PSI on top by cyclic voltammetry. Following Fig. 3B, *cyt c* exhibits a quasi-reversible electrochemistry with a formal potential of  $-8 \pm 4$  mV vs. Ag/AgCl ( $n = 8$ ), a small peak separation of  $12 \pm 2$  mV (at  $100$  mV s<sup>-1</sup>,  $n = 8$ ) and a surface coverage of  $14 \pm 0.8$  pmol cm<sup>-2</sup> ( $n = 8$ ). The data verify the

formation of a well-ordered *cyt c* ML and a fast electron transfer with the underlying electrode.

The subsequent adsorption of PSI on the *cyt c* ML can easily be recognized by a small potential shift towards lower potentials ( $-45 \pm 2$  mV vs. Ag/AgCl,  $n = 5$ ). The interaction of PSI with *cyt c* in a surface-fixed state obviously results in a stabilized oxidation state of *cyt c* compared to the reduced one. Despite the potential change the transferred charge remains almost constant verifying that all previously accessible *cyt c* molecules are still electro-active, additionally without detachment from surface. However, the broadening of the half peak-width ( $W_{0.5}$ ) of  $75 \pm 3$  mV ( $n = 4$ ) to  $83 \pm 3$  mV ( $n = 4$ ) indicates a change in the homogeneous state of the *cyt c* molecules in the monolayer to a slightly more heterogeneous one. After PSI deposition a change in the open circuit potential (OCP) can also be observed from 89 mV to 240 mV vs. Ag/AgCl. Although the measurements have been performed in the dark an absorption of residual light cannot be completely excluded, which could result in *cyt c* oxidation and thus a shift in OCP. In summary these observations indicate a strong interaction, such as *cyt c* binds to the luminal side of PSI, which may cause a

**Fig 3** Schematic electron flow in a *cyt c*/PSI assembly and photoelectrochemical experiments of Au-SAM/*cyt c*/PSI and Au-SAM/PSI: (A) After *cyt c* assembly on a MUA/MU-SAM PSI is deposited on the positively charged *cyt c* layer. Electrons can flow from the electrode via *cyt c* to PSI to reduce the reaction complex (P700<sup>+</sup>), when PSI is excited by light. A mediator (M) in solution oxidize the reduced F<sub>B</sub><sup>-</sup> iron sulfur cluster, which can be methyl viologen (MV<sup>2+</sup>) and oxygen. (B) Cyclic voltammogram of (a) Au-SAM/*cyt c* and (b) Au-SAM/*cyt c*/PSI electrodes in the dark and (c) Au-SAM/*cyt c*/PSI electrode under illumination of 60 mW cm<sup>-2</sup> white light. (C) Photocurrent density generated at two assemblies Au-SAM/PSI and Au-SAM/*cyt c*/PSI at -100 mV (black), +200 mV (red) and +500 mV (blue) vs. Ag/AgCl with corresponding current ratio (anodic to cathodic). Please note the current axis has been interrupted for better visualisation of the small photocurrents versus the *cyt c* mediated one. (D) chopped light voltammetry of Au-SAM/*cyt c*/PSI (a) without MV<sup>2+</sup> and (b) with MV<sup>2+</sup> illuminated with white light of a power of 60 mW cm<sup>-2</sup>. All measurements have been performed under aerobic conditions in phosphate buffer (5 mM, pH 7).

slight conformational change around the heme group, altering the redox properties.

When the *cyt c*/PSI electrode is illuminated with a light-power of 60 mW cm<sup>-2</sup> a catalytic current with still detectable oxidation and reduction peaks is observed (Fig. 3B). It needs to be pointed out, that catalysis is rather efficient here, since it can be observed even at a higher scan rate (100 mV s<sup>-1</sup>). The catalysis starts merely at the formal potential of *cyt c*, demonstrating that there is solely a photo-induced electron transfer from the electrode via *cyt c* to PSI, which reduces the positively charged P700<sup>+</sup>. This is schematically displayed in Fig. 3A.

Subsequently, the photocurrent has been measured at three different potentials (-100 mV, 200 mV and 500 mV vs. Ag/AgCl). The observations made are illustrated in Fig. 3C. Oxygen can oxidize the negatively charged iron-sulfur-cluster (F<sub>B</sub><sup>-</sup>) located at the stromal side of the PSI (and thus can act as electron acceptor "M<sup>+</sup>" as illustrated in Fig. 3A). A significant photocurrent of 1 μA cm<sup>-2</sup> can exclusively be observed at a negative polarization of the electrode (-100 mV vs. Ag/AgCl). At +500 mV vs. Ag/AgCl only a photocurrent of 13 nA cm<sup>-2</sup> is found, as well as 9 nA cm<sup>-2</sup> at +200 mV vs. Ag/AgCl, respectively. The ratio between anodic and cathodic photocurrents is calculated to be 0.014. This observation indicates a nearly unidirectional photocurrent generation, when PSI is assembled on a *cyt c* ML, emphasizing a rather well oriented PSI on the *cyt c* surface and a *cyt c*-mediated connection to the electrode.

To further evaluate the influence of *cyt c* on the photo-induced electron transport pathway a control electrode without *cyt c* has been prepared, taking into account that also other carboxy-modified electrodes have been reported for PSI assembly and photocurrent generation.<sup>14-19</sup> At a potential of -100 mV vs. Ag/AgCl such an electrode (Au-SAM/PSI) generates only a rather small photocurrent of about 17 nA cm<sup>-2</sup>. Additionally, a potential change to +500 mV vs. Ag/AgCl induces even smaller photocurrents, resulting in a ratio of anodic to cathodic current of 0.540. This clearly indicates that not only the magnitude of the photocurrent can be increased by the *cyt c* layer compared to the SAM approach, but also the proper orientation of immobilized PSI has been improved. Thus, the *cyt c*/PSI electrode can be considered as a biohybrid photodiode. Stability experiments of these electrodes reveal only about 20% loss in photo activity after 7 days stored at 4 °C in buffer.

In a next characterization step the potential dependence of the cathodic photocurrent has been evaluated. In Fig. 3D a chopped light voltammetric experiment of an Au/SAM/*cyt c*/PSI electrode is displayed. Obviously the photocurrents are enhanced by decreasing the applied potential. In pure buffer oxygen act as the electron acceptor in the system. Addition of the well-known electron acceptor MV<sup>2+</sup> leads to an increase of the photocurrent and improves the withdrawal of electrons from the excited PSI. Notwithstanding, MV<sup>2+</sup> is added to the solution, the potential dependence of the photocurrent is retained. The use of MV<sup>2+</sup> has the advantage of not displaying

any photochemical activity by itself or creating a shortcut with cyt *c*. Even though there is a strong  $MV^{2+}$  induced photocurrent enhancement at cathodic potentials, only tiny improvements are observed near the OCP. This observation is in accordance with the idea of a cyt *c* driven unidirectional assembly and the generation of an electron flow preferentially in one direction.

As a further characterization a light power dependence experiment without  $MV^{2+}$  has been performed with the Au-SAM/cyt *c*/PSI electrode (see Fig. s2B, ESI). In this case, already at low light intensities a fast rise in photocurrent is observed. The obtained curve is fitted with the Michaelis-Menten equation, an approach which has been proposed previously<sup>20</sup>, assuming photons as substrate for PSI. However, the obtained fit is not accurate for low intensities. From the fit parameters a maximum photocurrent density of  $0.97 \pm 0.01 \mu A cm^{-2}$  and a  $K_M$  of  $2.4 \pm 0.1 mW cm^{-2}$  can be derived.

### Photocurrent generation by a cyt *c*/PSI multilayer assembly

Fig 4 (A) Scheme of the alternating assembly process of cyt *c*/PSI multilayers using the layer-by-layer technique and photoelectrochemical experiments of (cyt *c*/PSI) multilayers: (B) cyclic voltammogram in the dark with (a) cyt *c* monolayer electrode (Au-SAM/cyt *c*), (b) cyt *c*/PSI electrode (Au-SAM/[cyt *c*/PSI]<sub>1</sub>) and (c) with a terminal cyt *c* layer on top of the cyt *c*/PSI electrode (Au-SAM/[cyt *c*/PSI]<sub>1</sub>/cyt *c*). (C) Photochronoamperometric measurements of each successively added layer at three different light power ( $2 mW cm^{-2}$ ,  $10 mW cm^{-2}$  and  $20 mW cm^{-2}$ ) with (a) Au-SAM, (b) Au-SAM/cyt *c*, (c) Au-SAM/[cyt *c*/PSI]<sub>1</sub>, (d) Au-SAM/[cyt *c*/PSI]<sub>2</sub> and (e) Au-SAM/[cyt *c*/PSI]<sub>2</sub>/cyt *c* electrodes. Measurements have been performed under aerobic conditions and in phosphate buffer (5 mM, pH 7).

Fig. 4B shows the cyclic voltammogram when cyt *c* is deposited on a cyt *c*/PSI electrode. The assembly process can readily be followed in the voltammetric analysis. Whereas the assembly of PSI on cyt *c* changes the potential of the underlying cyt *c* molecules as described before ( $-45 \pm 2 mV$  vs. Ag/AgCl,  $n = 5$ ), the subsequent assembly of cyt *c* on PSI results in a potential shift back to the positive direction ( $11 \pm 3 mV$  vs. Ag/AgCl,  $n = 5$ ) with a larger peak separation ( $16 \pm 3 mV$ ,  $n = 5$ ). In addition, the electro-active amount of cyt *c* is increased to  $28 \pm 3 pmol cm^{-2}$  ( $n = 5$ ). This demonstrates that the additionally deposited cyt *c* is in electrical contact with the electrode. The behavior can be explained by interprotein cyt *c*-cyt *c* electron exchange as already has been verified previously in cyt *c* multilayers.<sup>33,41,42</sup>

It also needs to be mentioned that a deposition of PSI on top of this layered system (Au-SAM/[cyt *c*/PSI]<sub>2</sub>) decreases the redox potential again ( $-2 \pm 4 mV$  vs. Ag/AgCl,  $n = 5$ ). This effect is not as strong as with PSI deposited on the first cyt *c* layer, however reproducibly detectable. A further assembly step of cyt *c* on top of this layered system (Au-SAM/[cyt *c*/PSI]<sub>2</sub>/cyt *c*) shifts the redox potential back to a more positive potential of  $16 \pm 3 mV$  vs. Ag/AgCl ( $n = 5$ ).

A functional analysis of the photocurrent generation with a successively assembled architecture of multiple layers (Au-SAM/[cyt *c*/PSI]<sub>1</sub>/cyt *c*) at  $-100 mV$  vs. Ag/AgCl reveals a clear increase in photocurrent density compared to the Au-SAM/cyt *c*/PSI system. The use of cyt *c* as a surface confined electron shuttle on top of the cyt *c*/PSI layer enhances the cathodic photocurrent additionally by at least 11 %, indicating that not all previously immobilized PSI molecules are in

In a next step of development we have tried to extend the idea of contacting PSI with the electrode by means of cyt *c*. In order to increase the surface concentration of PSI 3D protein architectures have been built up by applying the layer-by-layer deposition technique (see Fig. 4A). First assembly studies have been carried out by SPR in order to verify the formation of multilayered arrangements. Here, a fast adsorption of cyt *c* on a cyt *c*/PSI system can be observed. Subsequent injections of PSI also lead to a strong mass accumulation on the surface. It needs to be mentioned at this point that no further PSI deposition is possible after surface saturation is reached. Only on the basis of an intermittent cyt *c* adsorption further PSI deposition becomes feasible.

The formed multilayers (Au-SAM/[cyt *c*/PSI]<sub>*n*</sub>/cyt *c*,  $n = 1, 2$ ) have been studied electrochemically in order to test one important prerequisite – the electrical connectivity of cyt *c* within the different layers and the electrode.

electrical contact with the electrode. The additional cyt *c* molecules connect electrochemically some improperly orientated PSI molecules. Even higher photocurrents are generated when a two bilayer system with a terminal cyt *c* layer (Au-SAM/[cyt *c*/PSI]<sub>2</sub>/cyt *c*) is analyzed, as illustrated in Fig. 4C. The resulting photocurrent is increased by 40 %. Further experiments at positive potentials do not lead to a significant rise in anodic photocurrent density, which also supports the idea of a cyt *c* –based connection of the P700 complex in PSI with the electrode.

Even though the hybrid systems are assembled in a layer-by-layer fashion this does not result in well separated PSI and cyt *c* layers. Considering the size differences between PSI and cyt *c* and the observed photocurrent behavior of the multilayered electrode, it can be concluded that the cyt *c* molecules assemble around the PSI (i.e. on the accessible area of the PSI-complex). At this point it needs also to be stressed, that the terminal cyt *c* assembly is essential for a reasonable photocurrent since the two bilayer system of Au-SAM/[cyt *c*/PSI]<sub>2</sub> turns out to generate less photocurrent output (reduction of 30 %, see Fig. 4C). This observation is in agreement with the behavior found for a cyt *c* assembly on top of one bilayer system cyt *c*/PSI, which also results in an improved electrochemical connection of the large PSI complex with the electrode surface.

### Conclusions

In the present study we have demonstrated the possibility of electrochemically connecting photosystem I with an electrode transducer via the electron carrier protein cytochrome *c* on MUA/MU-modified gold surfaces. Assembly studies have elucidated the formation of a dense PSI layer on such *cyt c* electrodes and an enhanced protein deposition compared to electrodes with only a SAM-layer. A *cyt c*/PSI system clearly displays enhanced photocurrent densities and also leads to an unidirectional photocurrent generation indicating a *cyt c* driven orientation of PSI. A particular feature of this system can be seen in the finding that the process of assembly can be nicely followed via cyclic voltammetry, since the deposition of PSI changes the redox potential of *cyt c* noticeably.

Moreover, 3D architectures of *cyt c*/PSI have been accomplished based on the layer-by-layer deposition technique. In such multilayered systems, *cyt c* acts as a wiring agent between the separated PSI layers and the electrode. Owing to the well established communication between *cyt c* and the electrode and the high density of PSI molecules assembled on the electrode, rather large photocurrents have been achieved. This system highlights the importance of biomimetic approaches using natural building blocks to create artificial signal chains. It can also provide a biohybrid platform for the development of light driven enzyme cascades producing valuable chemical compounds.

### Acknowledgements

We gratefully acknowledge the support of this research by the Bundesministerium für Bildung und Forschung BMBF, Germany (Biotechnologie 2020+, projects: 031A154A+B) and BBSRC/EuroCores (BB/J00823011).

### Notes and references

<sup>a</sup> Biosystems Technology, Technical University of Applied Sciences Wildau, Hochschulring 1, D-15745 Wildau, Germany. E-mail: flisdat@th-wildau.de

<sup>b</sup> Institute for Molecular, Cell & Systems Biology, Glasgow Biomedical Research Centre, University of Glasgow, 120 University Place, Glasgow, G12 8TA, Scotland/UK.

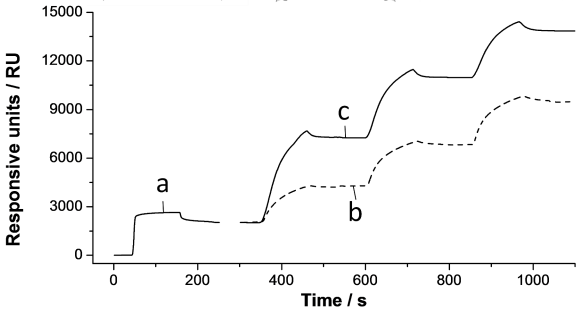
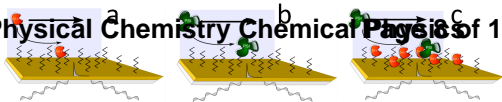
Electronic Supplementary Information (ESI) available: [details of any supplementary information available should be included here]. See DOI: 10.1039/b000000x/

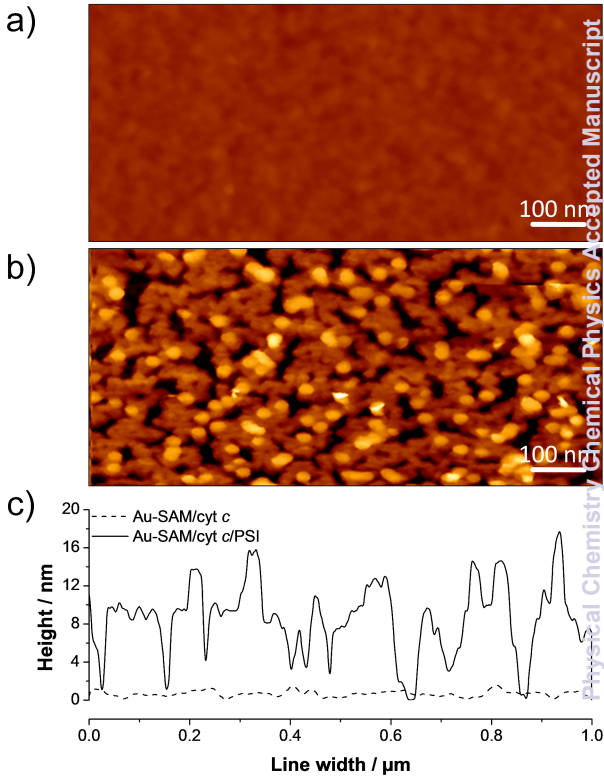
- 1 A. Badura, T. Kothe, W. Schuhmann and M. Rögner, *Energy Environ. Sci.*, 2011, **4**, 3263–3274.
- 2 F. Wang, X. Liu and I. Willner, *Adv. Mater.*, 2013, **25**, 349–377.
- 3 C. F. Meunier, X.-Y. Yang, J. C. Rooke and B.-L. Su, *ChemCatChem*, 2011, **3**, 476–488.
- 4 N. Nelson and C. F. Yocum, *Annu. Rev. Plant Biol.*, 2006, **57**, 521–565.
- 5 H. W. Trissl and C. Wilhelm, *Trends Biochem. Sci.*, 1993, **18**, 415.
- 6 I. Grotjohann and P. Fromme, *Photosynth. Res.*, 2005, **85** (1), 51–72.
- 7 A. Díaz-Quintana, W. Leibl, H. Bottin and P. Sétif, *Biochemistry*, 1998, **37** (10), 3429–3439.
- 8 P. Jordan, P. Fromme, H. T. Witt, O. Klukas, W. Saenger and N. Krauss, *Nature*, 2001, **411**, 909.
- 9 C. J. Faulkner, S. Lees, P. N. Ciesielski, D. E. Cliffel and G. K. Jennings, *Langmuir*, 2008, **24**, 8409–8412.
- 10 P. N. Ciesielski, A. M. Scott, C. J. Faulkner, B. J. Berron, D. E. Cliffel and G. K. Jennings, *ACS Nano*, 2008, **2**, 2465–72.
- 11 N. Terasaki, N. Yamamoto, T. Hiraga, I. Sato, Y. Inoue and S. Yamada, *Thin Solid Films*, 2006, **499**, 153–156.
- 12 N. Terasaki, N. Yamamoto, K. Tamada, M. Hattori, T. Hiraga, A. Tohri, I. Sato, M. Iwai, M. Iwai, S. Taguchi, I. Enami, Y. Inoue, Y. Yamanoi, T. Yonezawa, K. Mizuno, M. Murata, H. Nishihara, S. Yoneyama, M. Minakata, T. Ohmori, M. Sakai and M. Fujii, *Biochim. Biophys. Acta, Bioenerg.*, 2007, **1767**, 653–659.
- 13 O. Yehezkeili, O. I. Wilner, R. Tel-Vered, D. Roizman-Sade, R. Nechushtai and I. Willner, *J. Phys. Chem. B*, 2010, **114**, 14383–14388.
- 14 B. S. Ko, B. Babcock, G. K. Jennings, S. G. Tilden, R. R. Peterson, D. Cliffel and E. Greenbaum, *Langmuir*, 2004, **20** (10), 4033–4038.
- 15 H. A. Kincaid, T. Niedringhaus, M. Ciobanu, D. E. Cliffel and G. K. Jennings, *Langmuir*, 2006, **22**, 8114–20.
- 16 I. Carmeli, L. Frolov, C. Carmeli and S. Richter, *J. Am. Chem. Soc.*, 2007, **129**, 12352–3.
- 17 M. Ciobanu, H. A. Kincaid, V. Lo, A. D. Dukes, G. K. Jennings and D. E. Cliffel, *J. Electroanal. Chem.*, 2007, **599** (1), 72–78.
- 18 X. Yan, C. J. Faulkner, G. K. Jennings, and D. E. Cliffel, *Langmuir*, 2012, **28**, 15080–6.
- 19 A. K. Manocchi, D. R. Baker, S. S. Pendley, K. Nguyen, M. M. Hurlley, B. D. Bruce, J. J. Sumner and C. Lundgren, *Langmuir*, 2013, **29**, 2412–9.
- 20 A. Badura, D. Guschin, T. Kothe, M. J. Kopeczak, W. Schuhmann and M. Rögner, *Energy Environ. Sci.*, 2011, **4**, 2435–2440.
- 21 G. Chen, G. LeBlanc, G. K. Jennings, and D. E. Cliffel, *J. Electrochem. Soc.*, 2013, **160**, H315–H320.
- 22 K. Brettel and W. Leibl, *Biochim. Biophys. Acta*, 2001, **1507** (1–3), 100–14.
- 23 P. N. Ciesielski, D. E. Cliffel and G. K. Jennings, *J. Phys. Chem. A*, 2011, **115** (15), 3326–34.
- 24 C. A. Kerfeld and D. W. Krogmann, *Annu. Rev. Plant Physiol. Plant Mol. Biol.*, 1998, **49**, 397–425.
- 25 W. A. Cramer, H. Zhang, J. Yan, G. Kurisu and J. L. Smith, *Biochemistry*, 2004, **43**, 2921–2929.
- 26 A. Efrati, R. Tel-Vered, D. Michaeli, R. Nechushtai and I. Willner, *Energy Environ. Sci.*, 2013, **6**, 2950.
- 27 V. Proux-Delrouyre, C. Demaille, W. Leibl, P. Sétif, H. Bottin and C. Bourdillon, *Am. Chem. Soc.*, 2003, **125**, 13686–92.
- 28 L. Malmgren, Y. Olsson, T. Olsson and K. Kristensson, *Brain Res.*, 1978, **153**, 477–493.
- 29 S. Song, R. A. Clark, E. F. Bowden and M. Tarlov, *J. Phys. Chem.*, 1993, **97**, 6564–6572.
- 30 B. Ge and F. Lisdat, *Anal. Chim. Acta*, 2002, **454**, 53–64.
- 31 A. Avila, B. W. Gregory, K. Niki and T. M. Cotton, *J. Phys. Chem. B*, 2000, **104**, 2759–2766.
- 32 A. Efrati, O. Yehezkeili, R. Tel-Vered D. Michaeli, R. Nechushtai and I. Willner, *ACS Nano*, 2012, **6**, 9258–66.
- 33 M. K. Beissenhirtz, F. W. Scheller, W. F. M. Stöcklein, D. G. Kurth, H. Möhwald and F. Lisdat, *Angew. Chem. Int. Ed.*, 2004, **43**, 4357–4360.
- 34 A. T. Brunger, P. D. Adams, P. Fromme, R. Fromme, M. Levitt and G. F. Schroder, *Structure*, 2012, **20**, 957.
- 35 N.A. Baker, D. Sept, S. Joseph, M. J. Holst and J. A. McCammon, *Proc. Natl. Acad. Sci.*, 2001, **98**, 10037–10041.
- 36 M. Holst and F. Saied, *J. Comput. Chem.*, 1993, **14**, 105–133.
- 37 M. Holst and F. Saied, *J. Comput. Chem.*, 1995, **16**, 337–364.
- 38 F. Müh and A. Zouni, *Biochim. Biophys. Acta*, 2008, **1778**, 2298–307.
- 39 F. Müh and A. Zouni, *Biochim. Biophys. Acta*, 2005, **1708**, 219–28.
- 40 D. Mukherjee, M. Vaughn, B. Khomami and B. D. Bruce, *Colloids Surf. B. Biointerfaces*, 2011, **88**, 181–90.
- 41 F. Lisdat, R. Dronov, H. Möhwald, F.W. Scheller, D.G. Kurth, *Chem. Com* 3 (2009) 274–283
- 42 S.C. Feifel and F. Lisdat, *Journal of Nanobiotechnology*, 2011, **9**, 59.

43 O. Yehezkeli, R. Tel-Vered, D. Michaeli, R. Nechushtai and I. Willner, *Small*, 2013, **9**, 1–9.

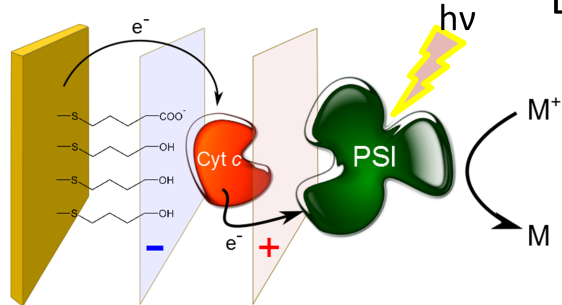
44 T. Kothe, N. Plumeré, A. Badura, M. M. Nowaczyk, D. Guschin, M. Rögner and W. Schuhmann, *Angew. Chem. Int. Ed. Engl.* 2013, **52**, 14233–6.

# Physical Chemistry Chemical Physics of 11

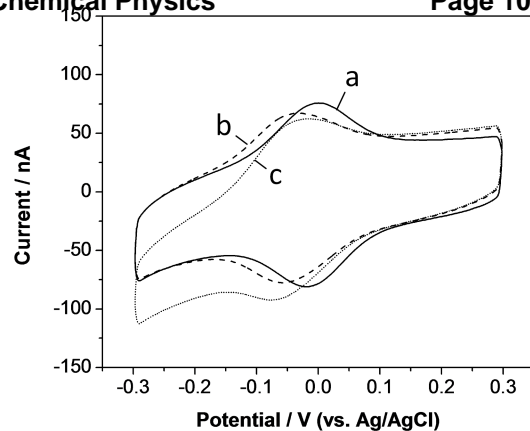




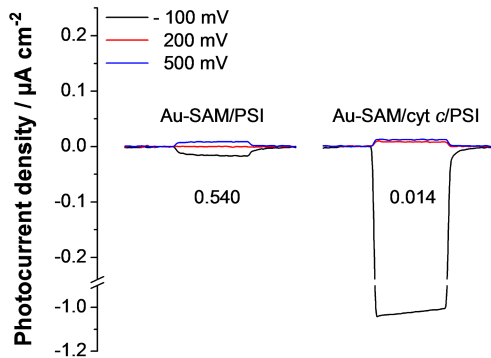
A



B



C



D

